

Switching-free time-domain optical quantum computation with quantum teleportation

Warit Asavanant,^{1,*} Kosuke Fukui,^{1,†} Atsushi Sakaguchi,^{2,‡} and Akira Furusawa^{1,2,§}

¹*Department of Applied Physics, School of Engineering,*

The University of Tokyo, 7-3-1 Hongo, Bunkyo-ku, Tokyo 113-8656, Japan

²*Optical Quantum Computing Research Team, RIKEN Center for Quantum Computing,*

2-1 Hirosawa, Wako, Saitama 351-0198, Japan

(Dated: February 3, 2022)

Optical switches and rerouting network are main obstacles to realize optical quantum computer. In particular, both components have been considered as essential components to the measurement-based time-domain optical quantum computation, which has seen promising developments regarding scalability in the recent years. Realizing optical switches and rerouting network with sufficient performance is, however, experimentally challenging as they must have extremely low loss, small switching time, high repetition rate, and minimum optical nonlinearity. In this work, we present an optical quantum computation platform that does not require such optical switches. Our method is based on continuous-variable measurement-based quantum computation, where instead of the typical cluster states, we modify the structure of the quantum entanglements, so that quantum teleportation protocol can be employed instead of the optical switching and rerouting. We also show that when combined with Gottesman-Kitaev-Preskill encoding, our architecture can outperform the architecture with optical switches when the optical losses of the switches are not low.

I. INTRODUCTION

Optical systems are promising candidates to realize quantum computation as they can be implemented at room temperature and atmospheric pressure, and have high compatibility with optical communications. Optical quantum computation can be largely categorized into two types: discrete variables (DV) and continuous variables (CV). Various researches have been done for both types and many different platforms have been theoretically developed and experimentally demonstrated [1, 2]. From these various platforms, time-domain CV measurement-based quantum computation [3] has shown a great potential regarding scalability: large-scale universal computational resource—the cluster state [4, 5]—has been generated [6–9] and basic operations on these scalable platform have also been demonstrated [10, 11].

Regardless of the details of each optical platform, optical switch is considered a key component. In the DV optical quantum computer, making a semi-deterministic single-photon source via multiplexing of probabilistic single-photon sources requires optical switches [12]. Also, tunable universal linear optics, which can be realized with optical switches and phase shifters, is essential when programming the DV optical quantum computer [13]. On the other hand, for the CV platforms—in particular, the measurement-based platform—optical switches are used in tasks such as the injection and dejection of the quantum states, injection of the magic states, error-correction circuits, and multiplexing of non-Gaussian ancillary states [14–17]. Despite the current development of

the optical switching for the optical quantum computer [14, 18], simultaneously realizing extremely low optical loss, high-speed switching, and high repetition rate remain highly challenging. For example, in a optical switch using pockel cell architecture which usually have low optical loss, voltage required in the switching is typically on the order of a few thousands volt, which limits the repetition rate. The repetition rate is especially important in the time-domain measurement-based architecture, where the inputs are encoded in a series of time-binned wave packets. In addition, as optical switching usually uses nonlinear optical medium, it is important to keep this nonlinearity from affecting the fragile quantum states. This can be challenging for some types of optical switches where high optical nonlinearity is required [19].

In this work, we present a switching-free CV measurement-based optical quantum computation platform in time domain. The main idea of this platform is that we appropriately modify the entanglement structure of the cluster states so that it can also function as optical switches and rerouting which are required when using the cluster states for quantum computation. This additional entanglement structure can be used for injection of the input state, multiplexing/rerouting of the ancillary state, and coupling of the cluster states to the ancillary states in the error syndrome measurement. We can select and switch between each function by switching the measurement bases of the homodyne measurement, allowing these functions to be implemented in via quantum teleportation protocol. This removes the necessity of the inline active optical components, and the required off-line active optical components are squeezed light sources and phase modulator for the local oscillators, which are both established technology [10, 11]. We also perform a numerical calculation showing that depending on the quality of the optical switches, our system can realize a lower error probability when combined with Gottesman-

* warit@alice.t.u-tokyo.ac.jp

† fukuik.opt@gmail.com

‡ atsushi.sakaguchi@riken.jp

§ akiraf@ap.t.u-tokyo.ac.jp

Kitaev-Preskill (GKP) encoding [20]. Although a similar concept can be seen in the fusion gate of the DV optical qubit [21], unlike the DV system, the CV entanglements are generated deterministically and continuously, making our approach experimentally viable. Therefore, this architecture removes the necessity of the optical switching from fault-tolerant universal optical quantum computation platform, making it unique compared to other time-domain CV architecture [8, 9, 16, 17].

This paper is structured as follows. Section II explains preliminaries and notations used in this paper. The proposed setup and its analysis are shown in Sec. III. Section IV discusses the experimental feasibility and shows the numerical analysis. Section V concludes the paper.

II. PRELIMINARIES

First we explain the basic notations and review the concepts of CV measurement-based quantum computation.

A. Notations

In CV quantum computation, the physical quantities of our interest are quadratures denoted by operators \hat{x} and \hat{p} which satisfy $[\hat{x}, \hat{p}] = i$ (we use the unit where $\hbar = 1$). The quadrature operators are related to annihilation operator \hat{a} and creation operator \hat{a}^\dagger via:

$$\hat{x} = \frac{1}{\sqrt{2}}(\hat{a} + \hat{a}^\dagger), \quad (1)$$

$$\hat{p} = -\frac{i}{\sqrt{2}}(\hat{a} - \hat{a}^\dagger). \quad (2)$$

Next, we define some of the basic operations in this paper. First, a squeezing operator $\hat{S}(r)$ with a squeezing parameter r transforms the quadrature operators in Heisenberg picture as

$$\hat{S}^\dagger(r) \begin{pmatrix} \hat{x} \\ \hat{p} \end{pmatrix} \hat{S}(r) = \begin{pmatrix} \hat{x} e^r \\ \hat{p} e^{-r} \end{pmatrix}. \quad (3)$$

Another important operation is a phase rotation $\hat{R}(\theta)$ which transforms quadrature operators as

$$\hat{R}^\dagger(\theta) \begin{pmatrix} \hat{x} \\ \hat{p} \end{pmatrix} \hat{R}(\theta) = \begin{pmatrix} \cos \theta & \sin \theta \\ -\sin \theta & \cos \theta \end{pmatrix} \begin{pmatrix} \hat{x} \\ \hat{p} \end{pmatrix}. \quad (4)$$

Regarding two-mode operation, we consider beamsplit-

ter interaction $\hat{B}_{12}(\sqrt{R})$ which we define as

$$\hat{B}_{12}^\dagger(\sqrt{R}) \begin{pmatrix} \hat{x}_1 \\ \hat{x}_2 \\ \hat{p}_1 \\ \hat{p}_2 \end{pmatrix} \hat{B}_{12}(\sqrt{R}) = \begin{pmatrix} \sqrt{R} & \sqrt{T} & 0 & 0 \\ -\sqrt{T} & \sqrt{R} & 0 & 0 \\ 0 & 0 & \sqrt{R} & \sqrt{T} \\ 0 & 0 & -\sqrt{T} & \sqrt{R} \end{pmatrix} \begin{pmatrix} \hat{x}_1 \\ \hat{x}_2 \\ \hat{p}_1 \\ \hat{p}_2 \end{pmatrix}. \quad (5)$$

B. Quantum entanglement and quantum computation

It is known that quantum entanglements with appropriate structures, i.e., the cluster states, allow universal quantum computation when combined with local (single mode or single qubit) measurements and feedforward operations that depend on the measurement results [4, 5]. Quantum computation using cluster states can be equivalently considered as sequential quantum teleportation where the measurement bases are chosen depending on the desired operations [6].

Quantum entanglement (and pure Gaussian states in general) in CV system is defined by a set of operators called nullifiers. For a N -mode pure Gaussian state $|G\rangle$, an operator $\hat{\delta}$ is a nullifier of $|G\rangle$ if and only if

$$\hat{\delta} |G\rangle = 0 \quad (6)$$

and the state $|G\rangle$ can be uniquely defined by N independent nullifiers.

In the generation of many ideal CV quantum entanglement, including the cluster states, infinite squeezing is required. In the actual physical situations, however, we can only achieve finite squeezing. The imperfections due to the finite squeezing appear as the non-zero variances of the nullifiers. When CV quantum entanglements are used, especially in measurement-based quantum computation, the squeezing of the nullifiers corresponds to the additional noises to the output, even when the quantum entanglement is not a pure Gaussian state [22]. The reason behind this is that the effects of the anti-squeezing components are erased by the feedforward operations. Therefore, when considering the CV quantum entanglements and their usage in measurement-based quantum computation, the variances of the nullifiers are the primary figures of merit.

C. Time-domain multiplexing method and macronodes

Figure 1 shows an experimental setup of the time-domain measurement-based quantum computation using a type of two-dimensional cluster states called quad-rail lattice [3]. In time-domain quantum computation, the

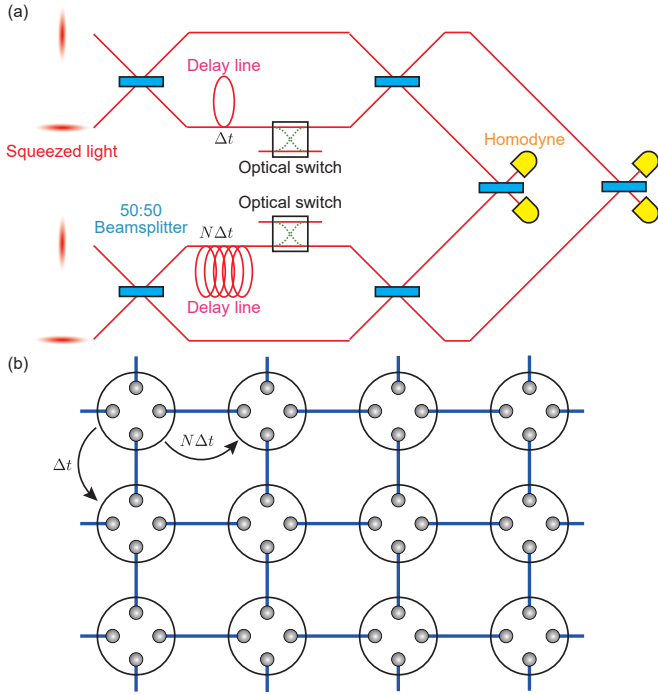


FIG. 1. Schematic diagram of time-domain-multiplexed quad-rail lattice cluster state setup. (a) The setup which consists of four squeezed light sources, five beamsplitters, four homodyne detectors, and optical switches. (b) Macronode representation of quad-rail lattice cluster state where the two-mode entanglement shown are two-mode squeezed state (EPR state in the infinite squeezing limit). Note that when considering quantum error correction, a switching for implementation of error correction is also required but it is omitted here [23].

modes of the cluster states are defined as a localized temporal wave packets in a time bin. By using two optical delay lines and linear optics, these wave packets are interfered resulting in the two-dimensional cluster state.

Although the quad-rail lattice cluster state can be reduced to conventional square-lattice cluster state via measurements and feedforward operations, a more efficient approach can be achieved by introducing the concept of macronodes; instead of the cluster state with complex structures, we can consider the operation on the quad-rail cluster state to be equivalent to quantum teleportation where the two-mode squeezed states are measured using a network of linear optics and homodyne measurement [24]. This same concept is also applied to other two-dimensional cluster states to achieve efficient quantum computation [23]. In the specific case of the quad-rail lattice cluster state, by choosing appropriate measurement bases, we can select between implementation of one-mode unitary operation on each input mode or interaction between two modes.

Although quantum computation using DV system does not require external input states as the nodes of the cluster states can be initialized as the inputs, for the CV state, the external input states is preferable as it usually

requires too many steps to make a complex state. State injection requires optical switch as shown in Fig. 1. In addition to the state injection, we also need the switching for the ancillary state used in error syndrome measurement and non-Gaussian measurement [15, 23]. These optical switches must have extremely low optical losses, high switching speed, and high repetition rate to be compatible with the time-domain multiplexing method.

III. MAIN RESULTS

A. Proposed setup

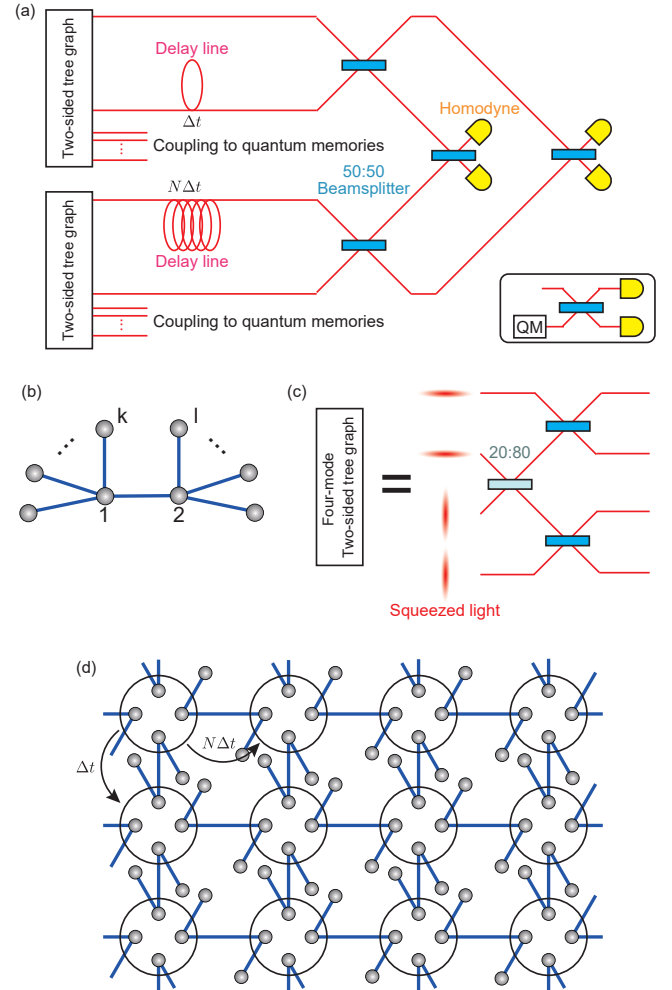


FIG. 2. Proposed switching-free optical quantum computer setup. (a) Experimental setup. The inset shows the coupling of the mode of the entanglement to the quantum memory (QM). (b) Two-sided tree graph state. (c) An example of the generation setup for the four-mode two-sided tree graph which is equivalent to four-mode linear cluster state. (d) Macronode representation of the setup. For simplicity, we show the case with four modes.

To circumvent the needs of the optical switching which

is a current bottle neck to the development of the optical quantum computer, we propose a setup shown in Fig. 2. In this setup, we replace the two-mode squeezed states in Fig. 1 with a CV quantum entanglement that has a tree-graph structure out branching out at both ends Fig. 1(b)]—which we will call *two-sided tree graph*. The nullifiers of the two-sided tree graph is given by

$$\hat{\delta}_1 = \hat{p}_1 - \hat{x}_2 - \sum_{k \in \mathcal{K}} \hat{x}_k, \quad (7)$$

$$\hat{\delta}_2 = \hat{p}_2 - \hat{x}_1 - \sum_{l \in \mathcal{L}} \hat{x}_l, \quad (8)$$

$$\hat{\delta}_k = \hat{p}_k - \hat{x}_1, \quad (9)$$

$$\hat{\delta}_l = \hat{p}_l - \hat{x}_2, \quad (10)$$

where \mathcal{K} (\mathcal{L}) is a set of nodes that is connected to mode 1 (2) and does not include mode 2 (1). Note that it is possible to transform this state into a state whose nullifiers composed of only quadrature operator \hat{x} or \hat{p} . Such type of state is the called \mathcal{H} -graph which can be generated via appropriate generalized parametric down conversion.

The branches of the two-sided tree graph are then coupled to a quantum memory via a 50:50 beamsplitter, where the mode 1 and 2 are inside the cluster circuit and is used for operations. Figure 2c shows an example of a possible generation setup of the two-sided tree graph in the four-mode case. This is the case with smallest number of modes and the resource state become a four-mode linear cluster states which have already been experimentally demonstrated [25]. For a case with more modes, it is theoretically shown that arbitrary Gaussian states can be generated with offline squeezing and linear optics [26], meaning that we can definitely find a physical circuit that realizes this initial resource state.

B. Input state injection and rerouting

In optical quantum computation, quantum states besides Gaussian states are usually generated using heralding method. Due to the random generation timing in the heralding method, the state generation is usually combined with quantum memories (For example, [27]). Then, optical switches are used to inject the generated states from the quantum memory into the cluster states. To increase the generation rate, it is expected that a network of quantum memories and rerouting system using optical switching would be required. Realizing this rerouting system with low optical losses is, however, technically difficult. Also, if the rerouting is slow, the required storage time of the optical memory will be longer which would degrade the state even more.

Here, we discuss how our proposed setup removes the need of the optical switches and rerouting network. The main idea is illustrated in Fig. 3 for a case with two quantum memories. First, two of the modes of the entanglement (the other two modes are used in the computa-

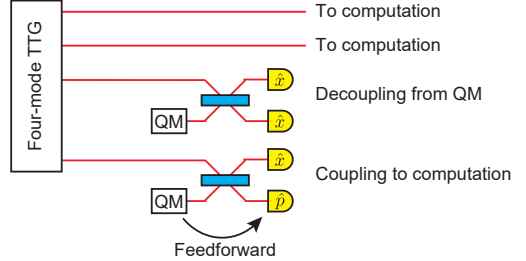


FIG. 3. State injection and rerouting with two-sided tree graph state. Here we show the case with four-mode two-sided tree graph (TTG), but this can be made arbitrary. When the state is generated and successfully stored in the quantum memory (QM), this information is used to feedforward to the measurement bases of the homodyne, and the quantum state is teleported as the input of our computation. The other quantum memories are decoupled to the computation by homodyne measurement of the same bases. Here we omitted the displacement operations that depend on the measurement results.

tion) are distributed and interfere on a 50:50 beamsplitter which is with the beam from the quantum memory, and a homodyne detector is put each output port of the beamsplitter. When we do not need to inject the quantum state, the measurement bases of all the homodyne detectors are set to \hat{x} . When the quantum state we wish to inject is successfully generated and stored inside one of the quantum memory, we use the quantum memory to adjust the timing and shift the measurement basis of one of the homodyne detectors to \hat{p} and teleport the state into the setup for further computation. The degree of freedom at the homodyne detectors for state injection can also be used to implement additional Gaussian operations if required [28]. Note, however, that the quantum memory is required when we consider continuous-wave optical generation of the non-Gaussian state, where the state generation usually occurs at a random timing. For a system where the generation timing is well-defined such as pulsed-laser system, we only require a fixed delay line to adjust the timing of feedforward operation. Comparing to the rerouting network, switching of the homodyne measurement basis is much easier as this is done by phase shifting of the local oscillator which is a classical light, meaning that we do not have to care about the optical losses in this case. Do note, however, that there will be trade-off as actual CV quantum entanglement can only be generated with finite squeezing and this will be discussed in Sec. IV. Similar to the state injection, we can also deject the state from the cluster state using a similar method where the branch of the additional entanglement is used as the output mode.

C. Universality

We also have to show the universality of our setup. In particular, universality on the GKP qubit is an aspect we need to consider as the GKP qubit is an important element for universal and fault-tolerant quantum computation with continuous variables [29–36]. Since the two-sided tree graph state can be reduced to a two-mode cluster state, the implementation of the Gaussian operations follows the protocol in Ref. [24] and can be done with homodyne measurements and feedforward operations.

On the other hand, there are several ways non-Gaussian operations can be implemented. The most basic way would be by replacing one of the homodyne detectors with nonlinear measurement such as cubic phase measurement [15]. This, however, requires optical switching to switch between the homodyne measurement and cubic phase measurement. As the cubic phase measurement utilize Gaussian operations and non-Gaussian ancillary state, we could instead use the entanglement structure of the two-sided tree graph and coupling the non-Gaussian ancillary states to the input states and then follow the measurement-based methodology to implement non-Gaussian gates [37].

If we consider GKP encoding, the Clifford operations can be implemented using Gaussian operations. On the other hand, non-Clifford operations required non-Gaussian operations [20]. Recently there has been a proposal where GKP non-Clifford operation is efficiently implemented using nonlinear feedforward system and ancillary state [38]. We can use the entanglement structure of the two-sided tree graph to couple the input with the ancillary state here and implement the adaptive homodyne measurement which results in the non-Clifford gate for GKP qubits after the feedforward operations. In this sense, the branches that are used for injection of the quantum state can also be used in the implementation of the non-Clifford operations.

D. Error syndrome measurement and correction

The quantum entanglement in our system can also be used for coupling the ancillary state with the logical qubit in the implementation of the error syndrome measurement in GKP qubit encoding. In our scheme, we use the Knill-type quantum error correction [39], where the data qubit is teleported to the fresh Bell state. The quantum error correction based on the Knill-type quantum error correction has been investigated in Refs. [35, 40]. In GKP Knill-type quantum error correction, error syndrome measurement and quantum error correction on GKP-encoded qubit can be done via quantum teleportation using GKP Bell state. In our current setup, if we generate GKP logical $|0_L\rangle$ or $|+_L\rangle$ and then inject it in from both end of the two-sided tree graph, the resulting entanglement will be GKP Bell pair as the injected states are joined by the controlled-Z gate after the tele-

portation.

Figure 4 shows the schematic diagram of the preparation of the GKP Bell state and quantum error correction based on quantum teleportation for our scheme. For the simplicity of the calculation, we consider the case where the two-sided tree graph state is prepared from two tree graph states via the Bell measurement (Fig 4(a)). Note that, in principle, direct preparation of the two-sided tree graph state is also possible with offline squeezing and linear optics [26]. To prepare the GKP Bell state, the GKP qubit from quantum memory is projected onto one mode of the Bell state, as shown in Fig 4(b), when the GKP qubit preparation succeeds in quantum memory. When the GKP qubit preparation fails in quantum memory, the measurement in the x quadrature is performed on the squeezed vacuum state corresponding the event for the failure of the GKP qubit preparation, as shown in Fig 4(c). Figure 4(d) shows the quantum error correction on the two data qubits 1 and 2 via quantum teleportation using the two GKP Bell pairs. In this step of error correction, the measurement bases are selected so that the two data qubits do not interact with each other and are teleported through different Bell pairs.

Moreover, as this GKP-Bell-pair teleportation can be implemented until succeeded, even if we manage to and generate and couple the GKP state to only one side of the two-sided tree graph, we can just try doing the error syndrome measurement and correction again until we succeeded. This property goes well with the heralding generation where the state generation occurs with randomly. Also, the success rate of this quantum error correction can be increased by increasing the number of branches and multiplexing the generation of GKP Bell pairs.

IV. EXPERIMENTAL FEASIBILITY AND NUMERICAL SIMULATION

To show the feasibility of our scheme, we numerically calculate the error probability of the controlled-Z gate on QRL. In QRL, the controlled-Z gate is followed by Fourier transformation, namely $\hat{F}\hat{F}\hat{C}\hat{Z}$ gate [23]. The error of the controlled-Z gate occurs when the GKP quantum error correction after $\hat{F}\hat{F}\hat{C}\hat{Z}$. To implement the GKP quantum error correction, the proposed method employs the GKP Bell state, while the conventional method with optical switches employs a quantum circuit with CZ gates which is used for the scheme proposed in Ref. [23].

The error probability of the GKP quantum error correction, P_{fail} , is calculated by

$$P_{\text{fail}} = 1 - \prod_{i=1}^4 (1 - E(\sigma_i)), \quad (11)$$

where $E(\sigma_i)$ corresponds to the probability of misidentifying the bit value of the GKP qubit i with the variance

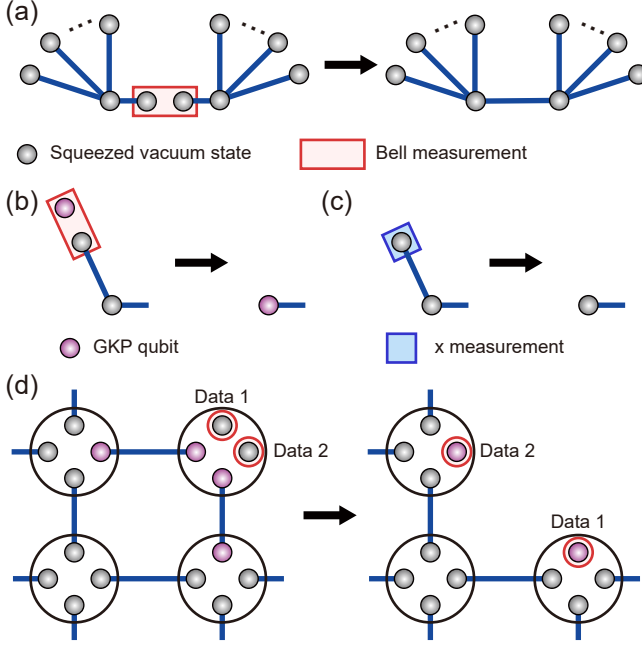


FIG. 4. The preparation of the GKP Bell state and quantum error correction based on quantum teleportation. (a) The preparation of two-sided tree graph state via the Bell measurement from two tree graph states. (b) The quantum teleportation of the GKP qubit on the one mode of the Bell state, where the GKP qubit preparation succeeds in quantum memory. (c) The disentanglement of the squeezed vacuum state with the Bell state by the measurement of the x measurement, where the GKP qubit preparation fails in quantum memory. (d) Quantum error correction of the two data qubits 1 and 2 via quantum teleportation using the two GKP Bell pairs.

σ_i^2 , and σ_i^2 depends on the effect of quantum gates, a photon loss of optical switchings, or the number of modes in two-sided graph state. The probability $E(\sigma)$ is obtained by

$$E(\sigma) = 1 - \sum_{k=-\infty}^{+\infty} \int_{2k\sqrt{\pi} - \frac{\sqrt{\pi}}{2}}^{2k\sqrt{\pi} + \frac{\sqrt{\pi}}{2}} dx \frac{1}{\sqrt{2\pi\sigma^2}} e^{-\frac{x^2}{2\sigma^2}} \quad (12)$$

For the setup with optical switches, σ_i^2 is equal to $\sigma_{g,i}^2 + \sigma_{n,i}^2 + \sigma_a^2$, where $\sigma_{g,i}^2$, $\sigma_{n,i}^2$, and $\sigma_{a,i}^2$ correspond to the transformation of variances of the input GKP qubit, the gate noise due to ancilla squeezed vacuums, and variance of ancilla GKP qubits for quantum error correction, respectively. For \hat{FFCZ} with the setup for QRL, the transformation of variances of the input state is equal to $2\sigma^2$ and σ^2 in the x and p quadratures, respectively, where σ^2 is the initial variance of the input GKP qubit. To calculate the error probability of \hat{FFCZ} gate, we set $\sigma_{g,i}^2$ as $\sigma_{g,1}^2 = \sigma_{g,2}^2 = 2\sigma'^2$ and $\sigma_{g,3}^2 = \sigma_{g,4}^2 = \sigma'^2$, where $\sigma'^2 = \sigma^2 + (1 - \eta)/\eta$ is the variance of the input state after a switching with efficiency η and the amplification. The variances $\sigma_{a,i}^2$ is set to $\sigma_{a,i}^2 = \sigma^2$. The

gate noise $\sigma_{n,i}^2$ becomes $\frac{1}{2}(1/2r_1^2 + 1)(2r_2)$, where r_1 and r_2 are the effective parameters for edge weight and self loops after switching loss (See Appendix for the details of r_1 and r_2). The effective parameters are obtained from $r_1 = \gamma\xi\tanh(2r)/\text{sech}(2r)$ and $r_2 = \sqrt{\gamma}\xi$ with the initial squeezing parameter of squeezed vacuums r , respectively, where γ and ξ are given by

$$\gamma = \frac{-\text{sech}(2r)^2 + \xi\sqrt{\xi^2 + 4\tanh^2(2r)/\text{sech}^2(2r)}}{2\xi^2\tanh^2(2r)/\text{sech}^2(2r)}, \quad (13)$$

$$\xi = \text{sech}(2r) + \frac{1 - \eta}{\eta}, \quad (14)$$

respectively.

For the proposed setup, σ_i^2 is equal to $\sigma_{g,i}^2 + \sigma_{n,i}^2 + \sigma_{a,i}^2$. We here assume the number of modes in the each side of two-sided tree graph as N . Then, the variances of the GKP Bell state in \hat{x} and \hat{p} quadratures are given by $(N + 2)\sigma^2$ and $(N + 3)\sigma^2$, respectively, and those of the squeezed vacuum Bell state are given by σ^2 and $(N + 3)\sigma^2$, respectively. The gate noise $\sigma_{n,i}^2$ is given by $(N + 4)\sigma^2$ for all i . We set $\sigma_{a,i}^2$ to $\sigma_{g,1}^2 = \sigma_{g,2}^2 = (N + 2)\sigma^2$ and $\sigma_{g,3}^2 = \sigma_{g,4}^2 = (N + 3)\sigma^3$,

Figure 5 (a) shows the error probability of \hat{FFCZ} gate with switching-free setup for several N which is numbers of modes in the each side of two-sided tree graph. In our setup, we set the number N to realize near deterministic preparation of the GKP Bell pair for quantum error correction. For example, the success probability of the GKP Bell pair preparation 99.99% can be achieved by setting $N=5, 10, 15$, and 20 for the success probabilities of the GKP qubit preparation in quantum memory 94.5, 73.5, 56.0, and 45.5%, respectively. For fault-tolerant quantum computation, we assume that fault-tolerant quantum computation can be realized if the error probability of \hat{FFCZ} is less than around 1%. Figure 5 (a) implies that our method provides fault-tolerant quantum computation even if large N . In Fig. 5 (b), to verify our scheme, we also plotted the error probability of \hat{FFCZ} gate with the conventional method with optical switches for several photon loss parameters $1 - \eta$. Note that although we also need to reduce the optical losses in our setup, the numerical results imply that fault-tolerant quantum computation using the method with optical switches will be difficult when $1 - \eta$ is slightly more than 1% since the error probability of \hat{FFCZ} is generally assumed to be around 1% to realize fault-tolerant quantum computation.

Regarding the experimental feasibility, despite the fact that it is possible to make a free-space optical switch with bulk optics where the losses are limited mainly by the quality of the anti-reflection coating, free-space optics are not a good choice when considering long term stability, reproducibility, and integratability. This is especially true when we consider the routing network for the non-Gaussian ancillary state, where the routing network would comprise of multiple optical switches. For

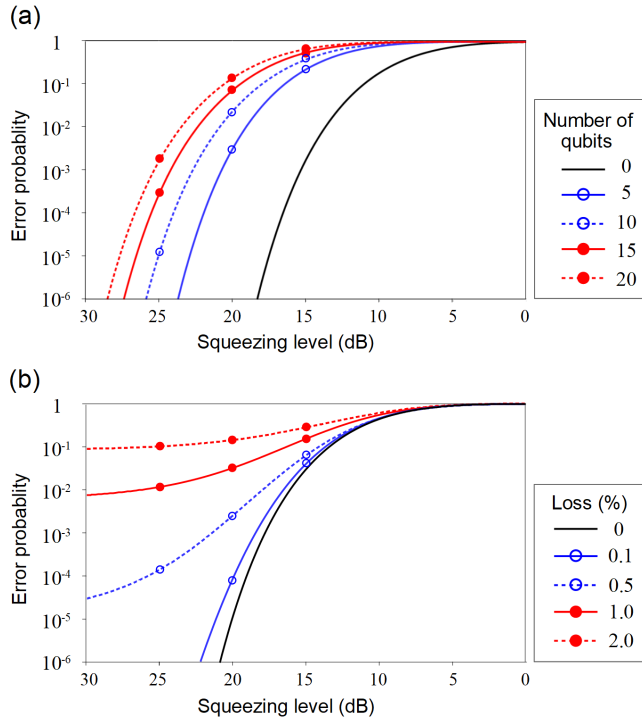


FIG. 5. The error probability of \hat{FFCZ} gate. (a) The proposed method with switching-free setup. (b) The conventional method for QRL with optical switches for several loss parameters of the optical switch.

the integrated optics such as silicon photonics, the optical losses are still too high for the quantum applications [41].

On the other hand, in the approach of using entanglement in this work, the CV quantum entanglement can be generated using only offline squeezed lights and passive linear optics and the switching of the measurement bases are done by changing the phases of the classical local oscillators which do not have the severe requirements regarding optical losses. In principle, the generation of the required quantum entanglement in time domain with sufficient quality is possible by extending the technology used in the cluster state generation and computation [8–11] and inclusion of high-quality squeezed light source [42]. Regarding the preparation of the GKP qubit which is required in most of the optical quantum computation architecture, although there are recent realizations in ion-trapped system [43] and superconducting system [44] and the optical generation has not been achieved yet, there are a few promising theoretical proposals (see, for example Ref. [45–47]). Also, development of optical quantum memory capable of storing multiphoton quantum state such as GKP state is being developed [27, 48].

V. CONCLUSION

We have presented an optical quantum computation platform which removes the necessity of the optical switches. Our approach incorporates the possibility of multiplexing of multiple non-Gaussian ancillary state generators and quantum memories by using the quantum teleportation protocol via two-sided tree graph states. The physical realization of our system is also highly scalable as it is compatible with the time-domain multiplexing methodology, and the only active components necessary is the phase modulation of the local oscillators which are relatively easy as modulation of classical light is a well-established technology. Hence, this architecture shows a possibility of efficient optical quantum architecture that does not require inline optical switching.

ACKNOWLEDGMENTS

This work was partly supported by JST [Moonshot R&D][Grant No. JPMJMS2064], JSPS KAKENHI (Grant No. 18H05207), UTokyo Foundation, and donations from Nichia Corporation.

Appendix A: Rescaling self-loop and edge-weight parameters

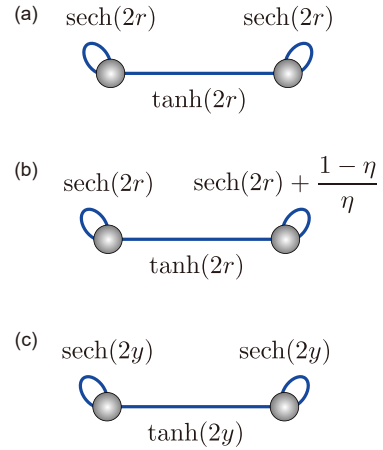


FIG. 6. Rescaling edge weight of the entangled pair. (a) Parameters for the edge weight $\tanh(2r)$ and self loop $\sinh(2r)$ for the entangled pair with the initial squeezing parameter r . (b) After photon loss and the amplification on one of the entangled pair with transmittance efficiency η . (c) After rescaling the parameters. Two self loops are equal to $\text{sech}(2y)$.

We describe the calculation for the details of r_1 and r_2 in the main text. In the scheme with optical switches in Fig. 1, where the self-loop and edge-weight parameters are $\text{sech}(2r)$ and $\tanh(2r)$, respectively, as shown in Fig. 6(a). One of entangled pair of squeezed vacuum state

suffers from photon loss by an optical switch, and the amplification is performed on the pair. Then the self-loop parameter for one of the entangled pair is transformed as

$$\operatorname{sech}(2r) \mapsto \operatorname{sech}(2r) + \frac{1-\eta}{\eta} \quad (\text{A1})$$

with the initial parameter r and transmittance efficiency η , as shown in Fig. 6(b). For the scheme based on the macro node protocol, the self-loop parameters for entangled pair need to be same, and thus we rescale the edge weight for the entangled pair as

$$\sqrt{\gamma_a \gamma_b} \tanh(2r) = \tanh(2y) \quad (\text{A2})$$

with the rescaled parameter y , as shown in Fig. 6(c). The rescaled parameters are transformed as

$$\operatorname{sech}(2r) \mapsto \sqrt{\gamma_a} \operatorname{sech}(2r), \quad (\text{A3})$$

$$\operatorname{sech}(2r) + \frac{1-\eta}{\eta} \mapsto \sqrt{\gamma_b} \left\{ \operatorname{sech}(2r) + \frac{1-\eta}{\eta} \right\}. \quad (\text{A4})$$

Then we set two above values to be equal as

$$\sqrt{\gamma_a} \operatorname{sech}(2r) = \sqrt{\gamma_b} \left\{ \operatorname{sech}(2r) + \frac{1-\eta}{\eta} \right\} = \operatorname{sech}(2y), \quad (\text{A5})$$

, as shown in Fig. 6(c). From $\operatorname{sech}^2(2y) + \tanh^2(2y) = 1$ with Eqs. (A2) and (A5), we obtain $\gamma = \gamma_b$ for Eq. (13) in the main text.

[1] S. Takeda and A. Furusawa, Toward large-scale fault-tolerant universal photonic quantum computing, *APL Photonics* **4**, 060902 (2019), <https://doi.org/10.1063/1.5100160>.

[2] S. Slussarenko and G. J. Pryde, Photonic quantum information processing: A concise review, *Applied Physics Reviews* **6**, 041303 (2019), <https://doi.org/10.1063/1.5115814>.

[3] N. C. Menicucci, Temporal-mode continuous-variable cluster states using linear optics, *Phys. Rev. A* **83**, 062314 (2011).

[4] R. Raussendorf and H. J. Briegel, A one-way quantum computer, *Phys. Rev. Lett.* **86**, 5188 (2001).

[5] N. C. Menicucci, P. van Loock, M. Gu, C. Weedbrook, T. C. Ralph, and M. A. Nielsen, Universal quantum computation with continuous-variable cluster states, *Phys. Rev. Lett.* **97**, 110501 (2006).

[6] S. Yokoyama, R. Ukai, S. C. Armstrong, C. Sornphiphatphong, T. Kaji, S. Suzuki, J. Yoshikawa, H. Yonezawa, N. C. Menicucci, and A. Furusawa, Ultra-large-scale continuous-variable cluster states multiplexed in the time domain, *Nature Photonics* **7**, 982 (2013).

[7] J. Yoshikawa, S. Yokoyama, T. Kaji, C. Sornphiphatphong, Y. Shiozawa, K. Makino, and A. Furusawa, Invited article: Generation of one-million-mode continuous-variable cluster state by unlimited time-domain multiplexing, *APL Photonics* **1**, 060801 (2016), <https://doi.org/10.1063/1.4962732>.

[8] W. Asavanant, Y. Shiozawa, S. Yokoyama, B. Charoensombutamon, H. Emura, R. N. Alexander, S. Takeda, J. Yoshikawa, N. C. Menicucci, H. Yonezawa, and A. Furusawa, Generation of time-domain-multiplexed two-dimensional cluster state, *Science* **366**, 373 (2019).

[9] M. V. Larsen, X. Guo, C. R. Breum, J. S. Neergaard-Nielsen, and U. L. Andersen, Deterministic generation of a two-dimensional cluster state, *Science* **366**, 369 (2019).

[10] W. Asavanant, B. Charoensombutamon, S. Yokoyama, T. Ebihara, T. Nakamura, R. N. Alexander, M. Endo, J. Yoshikawa, N. C. Menicucci, H. Yonezawa, and A. Furusawa, Time-domain-multiplexed measurement-based quantum operations with 25-MHz clock frequency, *Phys. Rev. Applied* **16**, 034005 (2021).

[11] M. V. Larsen, X. Guo, C. R. Breum, J. S. Neergaard-Nielsen, and U. L. Andersen, Deterministic multi-mode gates on a scalable photonic quantum computing platform, *Nature Physics* **17**, 1018 (2021).

[12] E. Meyer-Scott, C. Silberhorn, and A. Migdall, Single-photon sources: Approaching the ideal through multiplexing, *Review of Scientific Instruments* **91**, 041101 (2020), <https://doi.org/10.1063/5.0003320>.

[13] J. Carolan, C. Harrold, C. Sparrow, E. Martín-López, N. J. Russell, J. W. Silverstone, P. J. Shadbolt, N. Matsuda, M. Oguma, M. Itoh, G. D. Marshall, M. G. Thompson, J. C. F. Matthews, T. Hashimoto, J. L. O’Brien, and A. Laing, Universal linear optics, *Science* **349**, 711 (2015).

[14] M. V. Larsen, X. Guo, C. R. Breum, J. S. Neergaard-Nielsen, and U. L. Andersen, Fiber-coupled EPR-state generation using a single temporally multiplexed squeezed light source, *npj Quantum Information* **5**, 46 (2019).

[15] R. N. Alexander, S. Yokoyama, A. Furusawa, and N. C. Menicucci, Universal quantum computation with temporal-mode bilayer square lattices, *Phys. Rev. A* **97**, 032302 (2018).

[16] S. Takeda and A. Furusawa, Universal quantum computing with measurement-induced continuous-variable gate sequence in a loop-based architecture, *Phys. Rev. Lett.* **119**, 120504 (2017).

[17] M. V. Larsen, C. Chamberland, K. Noh, J. S. Neergaard-Nielsen, and U. L. Andersen, Fault-tolerant continuous-variable measurement-based quantum computation architecture, *PRX Quantum* **2**, 030325 (2021).

[18] S. Takeda, K. Takase, and A. Furusawa, On-demand photonic entanglement synthesizer, *Science Advances* **5**, eaaw4530 (2019).

[19] W. Yoshiki and T. Tanabe, All-optical switching using kerr effect in a silica toroid microcavity, *Opt. Express* **22**, 24332 (2014).

[20] D. Gottesman, A. Kitaev, and J. Preskill, Encoding a qubit in an oscillator, *Phys. Rev. A* **64**, 012310 (2001).

[21] D. E. Browne and T. Rudolph, Resource-efficient linear optical quantum computation, *Phys. Rev. Lett.* **95**, 010501 (2005).

[22] B. W. Walshe, L. J. Mensen, B. Q. Baragiola, and N. C. Menicucci, Robust fault tolerance for continuous-variable cluster states with excess antisqueezing, *Phys. Rev. A* **100**, 010301 (2019).

[23] M. V. Larsen, J. S. Neergaard-Nielsen, and U. L. Andersen, Architecture and noise analysis of continuous-variable quantum gates using two-dimensional cluster states, *Phys. Rev. A* **102**, 042608 (2020).

[24] R. N. Alexander and N. C. Menicucci, Flexible quantum circuits using scalable continuous-variable cluster states, *Phys. Rev. A* **93**, 062326 (2016).

[25] M. Yukawa, R. Ukai, P. van Loock, and A. Furusawa, Experimental generation of four-mode continuous-variable cluster states, *Phys. Rev. A* **78**, 012301 (2008).

[26] P. van Loock, C. Weedbrook, and M. Gu, Building gaussian cluster states by linear optics, *Phys. Rev. A* **76**, 032321 (2007).

[27] Y. Hashimoto, T. Toyama, J. Yoshikawa, K. Makino, F. Okamoto, R. Sakakibara, S. Takeda, P. van Loock, and A. Furusawa, All-optical storage of phase-sensitive quantum states of light, *Phys. Rev. Lett.* **123**, 113603 (2019).

[28] R. Ukai, J. Yoshikawa, N. Iwata, P. van Loock, and A. Furusawa, Universal linear bogoliubov transformations through one-way quantum computation, *Phys. Rev. A* **81**, 032315 (2010).

[29] N. C. Menicucci, Fault-tolerant measurement-based quantum computing with continuous-variable cluster states, *Phys. Rev. Lett.* **112**, 120504 (2014).

[30] B. Q. Baragiola, G. Pantaleoni, R. N. Alexander, A. Karanjai, and N. C. Menicucci, All-gaussian universality and fault tolerance with the gottesman-kitaev-preskill code, *Phys. Rev. Lett.* **123**, 200502 (2019).

[31] G. Pantaleoni, B. Q. Baragiola, and N. C. Menicucci, Modular bosonic subsystem codes, *Phys. Rev. Lett.* **125**, 040501 (2020).

[32] K. Fukui, A. Tomita, and A. Okamoto, Analog quantum error correction with encoding a qubit into an oscillator, *Phys. Rev. Lett.* **119**, 180507 (2017).

[33] K. Fukui, A. Tomita, A. Okamoto, and K. Fujii, High-threshold fault-tolerant quantum computation with analog quantum error correction, *Phys. Rev. X* **8**, 021054 (2018).

[34] K. Fukui, High-threshold fault-tolerant quantum computation with the GKP qubit and realistically noisy devices, arXiv e-prints , arXiv:1906.09767 (2019), arXiv:1906.09767 [quant-ph].

[35] B. W. Walshe, B. Q. Baragiola, R. N. Alexander, and N. C. Menicucci, Continuous-variable gate teleportation and bosonic-code error correction, *Phys. Rev. A* **102**, 062411 (2020).

[36] K. Noh and C. Chamberland, Fault-tolerant bosonic quantum error correction with the surface-gottesman-kitaev-preskill code, *Phys. Rev. A* **101**, 012316 (2020).

[37] P. Marek, R. Filip, H. Ogawa, A. Sakaguchi, S. Takeda, J. Yoshikawa, and A. Furusawa, General implementation of arbitrary nonlinear quadrature phase gates, *Phys. Rev. A* **97**, 022329 (2018).

[38] S. Konno, W. Asavanant, K. Fukui, A. Sakaguchi, F. Hanamura, P. Marek, R. Filip, J. Yoshikawa, and A. Furusawa, Non-clifford gate on optical qubits by non-linear feedforward, *Phys. Rev. Research* **3**, 043026 (2021).

[39] E. Knill, Scalable quantum computing in the presence of large detected-error rates, *Physical Review A* **71**, 042322 (2005).

[40] B. W. Walshe, R. N. Alexander, N. C. Menicucci, and B. Q. Baragiola, Streamlined quantum computing with macronode cluster states, *Phys. Rev. A* **104**, 062427 (2021).

[41] K. Suzuki, R. Konoike, S. Suda, H. Matsuura, S. Namiki, H. Kawashima, and K. Ikeda, Low-loss, low-crosstalk, and large-scale optical switch based on silicon photonics, *J. Lightwave Technol.* **38**, 233 (2020).

[42] H. Vahlbruch, M. Mehmet, K. Danzmann, and R. Schnabel, Detection of 15 dB squeezed states of light and their application for the absolute calibration of photoelectric quantum efficiency, *Phys. Rev. Lett.* **117**, 110801 (2016).

[43] C. Flühmann, T. L. Nguyen, M. Marinelli, V. Negnevitsky, K. Mehta, and J. P. Home, Encoding a qubit in a trapped-ion mechanical oscillator, *Nature* **566**, 513 (2019).

[44] P. Campagne-Ibarcq, A. Eickbusch, S. Touzard, E. Zalys-Geller, N. E. Frattini, V. V. Sivak, P. Reinhold, S. Puri, S. Shankar, R. J. Schoelkopf, L. Frunzio, M. Mirrahimi, and M. H. Devoret, Quantum error correction of a qubit encoded in grid states of an oscillator, *Nature* **584**, 368 (2020).

[45] I. Tzitrin, J. E. Bourassa, N. C. Menicucci, and K. K. Sabapathy, Progress towards practical qubit computation using approximate gottesman-kitaev-preskill codes, *Phys. Rev. A* **101**, 032315 (2020).

[46] K. Fukui, S. Takeda, M. Endo, W. Asavanant, J. Yoshikawa, P. van Loock, and A. Furusawa, Efficient backcasting search for optical quantum state synthesis, arXiv e-prints , arXiv:2109.01444 (2021), arXiv:2109.01444 [quant-ph].

[47] K. Fukui, M. Endo, W. Asavanant, A. Sakaguchi, J. Yoshikawa, and A. Furusawa, Generating Gottesman-Kitaev-Preskill qubit using a cross-Kerr interaction between a squeezed light and Fock states in optics, arXiv e-prints , arXiv:2109.04801 (2021), arXiv:2109.04801 [quant-ph].

[48] J. Yoshikawa, K. Makino, S. Kurata, P. van Loock, and A. Furusawa, Creation, storage, and on-demand release of optical quantum states with a negative wigner function, *Phys. Rev. X* **3**, 041028 (2013).